Johann Radon Institute for
Computational and Applied Mathematics
Austrian Academy of Sciences (ÖAW)

Algebraic multigrid for finite element elasticity equations: Determination of nodal dependence via edge matrices and two-level convergence

E. Karer, J. Kraus

RICAM-Report 2009-02

Algebraic multigrid for finite element elasticity equations: Determination of nodal dependence via edge matrices and two-level convergence

E. Karer J. K. Kraus

Abstract

We study an algebraic multigrid (AMG) method for solving elliptic finite element equations of linear elasticity problems. In this method, which has been proposed in [J.K. Kraus, *SIAM J. Sci. Comput.*, 30 (2008), pp. 505–524], the coarsening is based on so-called edge matrices, which allows to generalize the concept of strong and weak connections, as used in classical AMG, to "algebraic vertices" that accumulate the nodal degrees of freedom in case of vector-field problems. The major contribution of this work is related to the investigation of the measure for the nodal dependence and on the generation of the edge matrices, which are the basic building blocks of this method. A natural measure is the cosine of the abstract angle between the two subspaces spanned by the basis functions corresponding to the respective algebraic vertices. Another original contribution of this work is a two-level convergence analysis of the method. The presented numerical results cover also problems with jumps in the Young's modulus of elasticity and orthotropic materials.

1 Introduction

We are concerned with the solution of large-scale systems of linear equations

$$A\mathbf{x} = \mathbf{b} \tag{1}$$

arising from first-order finite element discretization of linear elasticity problems. In this case the system matrix A is symmetric and positive definite (SPD). It is well known that algebraic multigrid (AMG) methods can serve as efficient linear solvers or preconditioners for this type of problems. Especially two classes of methods, namely AMG using element interpolation (AMGe), see, e.g., [3, 9, 10], and AMG based on smoothed aggregation [18, 19], provide powerful solution tools. Recently, a variant of AMGe, called algebraic multigrid based on computational molecules (AMGm), has been proposed by one of the authors [13], see also [14]. The goal of this modification of AMGe is to combine the favorable properties of classical AMG [20], such as an inexpensive set-up phase due to a simple coarsening procedure based on strong connections, with the superior convergence properties of AMGe, which are achieved by local harmonic interpolation.

A basic step in the construction of this method, is the computation of so-called "edge matrices", which represent the nodal dependence, and, when assembled globally, define a spectrally equivalent auxiliary problem. This auxiliary problem determines the coarsening process. Our approach originates in so-called element preconditioning techniques first introduced in [8, 15]. The computation of edge matrices has initially been considered in [14] for scalar problems, and has then been generalized to problems in linear elasticity in Reference [13].

In the present paper we offer an alternative way to compute edge matrices in linear elasticity that improves the approximation properties of the auxiliary problem. Moreover, we

propose a natural measure for the strength of nodal dependence defined via the constant in the strengthened Cauchy-Bunyakowski-Schwarz inequality associated with local (vertex) subspaces, and provide a two-level convergence analysis of the obtained AMGm method. Towards the end of the paper we present several numerical experiments summarizing convergence results for reference configurations of three-dimensional bodies, including the cases of orthotropic materials, e.g., cancellous bone, hard wood, or soft wood, and problems with jumps in the Young's modulus of elasticity.

2 Problem

As noted above, we are dealing with problems arising in linear elasticity. Therefore, let Ω be a bounded, connected and open subset of $\mathbb{R}^d$, $d = 2, 3$, denoting the reference configuration of an elastic body. The boundary of Ω is divided into two disjoint parts Γ_0 and Γ_1, i.e., $\bar{\Gamma}_0 \cup \bar{\Gamma}_1 = \partial\Omega$ and $\Gamma_0 \cap \Gamma_1 = \emptyset$. From the theory of linear elasticity (see [2] for instance) it is well known that the governing equations of our problem are given by

$$-\operatorname{div} \boldsymbol{\sigma} = \mathbf{f} \qquad \text{in } \Omega, \tag{2a}$$

$$\mathbf{u} = \mathbf{0} \qquad \text{on } \Gamma_0, \tag{2b}$$

$$\boldsymbol{\sigma} \cdot \mathbf{n} = \mathbf{g} \qquad \text{on } \Gamma_1. \tag{2c}$$

These equations describe the deformation of the body under the influence of body and surface forces. Thereby only first-order terms of the displacement are taken into account. In this system, $\boldsymbol{\sigma}$ denotes the stress tensor, $\mathbf{f}$ the body forces, and $\mathbf{u}$ the displacements. Moreover, $\mathbf{n}$ denotes the outwards pointing unit normal vector on $\partial\Omega$ and $\mathbf{g}$ the applied load on Γ_1. Additionally to the Neumann-boundary conditions we fix the displacement $\mathbf{u}$ at Γ_0 in order to guarantee the uniqueness of the solution.

Writing the stress tensor $\boldsymbol{\sigma}$ and the strain tensor $\boldsymbol{\varepsilon}$ in vector form, that is $\boldsymbol{\sigma} = (\sigma_{11}, \sigma_{22}, \sigma_{33}, \sigma_{12}, \sigma_{13}, \sigma_{23})^T$ and $\boldsymbol{\varepsilon} = (\varepsilon_{11}, \varepsilon_{22}, \varepsilon_{33}, 2\varepsilon_{12}, 2\varepsilon_{13}, 2\varepsilon_{23})^T$ we obtain the stress-strain relation by Hooke's law, i.e., $\boldsymbol{\sigma} = C_{\text{iso}} \cdot \boldsymbol{\varepsilon}$. For St. Vernant-Kirchhoff-materials (homogeneous and isotropic) the stress-strain matrix C_{iso} is defined by

$$C_{\text{iso}}^{-1} := \begin{pmatrix} 1/E & -\nu/E & -\nu/E & 0 & 0 & 0 \\ -\nu/E & 1/E & -\nu/E & 0 & 0 & 0 \\ -\nu/E & -\nu/E & 1/E & 0 & 0 & 0 \\ 0 & 0 & 0 & 1/\mu & 0 & 0 \\ 0 & 0 & 0 & 0 & 1/\mu & 0 \\ 0 & 0 & 0 & 0 & 0 & 1/\mu \end{pmatrix}, \tag{3}$$

with the modulus of elasticity E, the Poisson ratio ν and the shear modulus $\mu := \frac{E}{2(1+\nu)}$. We further introduce the Lamé constant $\lambda := \frac{E\nu}{(1+\nu)(1-2\nu)}$ and the symmetric gradient $\nabla^{(s)}\mathbf{u} := \boldsymbol{\varepsilon}(\mathbf{u})$ with $\varepsilon_{ij}(\mathbf{u}) = \frac{1}{2}\left(\frac{\partial u_i}{\partial x_j} + \frac{\partial u_j}{\partial x_i}\right)$. Then, (2a) yields the classical Lamé differential equation

$$-2\mu \operatorname{div} \nabla^{(s)}\mathbf{u} - \lambda \operatorname{grad} \operatorname{div} \mathbf{u} = \mathbf{f}. \tag{4}$$

Hence, we end up with the following weak formulation of the boundary-value problem (2a)-(2c): Find $\mathbf{u} \in V = V(\Omega) := \{\mathbf{v} \in [H^1(\Omega)]^d : \mathbf{v} = \mathbf{0} \text{ on } \Gamma_0\}$ such that

$$a(\mathbf{u}, \mathbf{v}) = L(\mathbf{v}) \qquad \forall \mathbf{v} \in V \tag{5}$$

with

$$a(\mathbf{u}, \mathbf{v}) = a_{\text{iso}}(\mathbf{u}, \mathbf{v}) := 2\mu(\nabla^{(s)}\mathbf{u}\,, \nabla^{(s)}\mathbf{v}) + \lambda\,(\operatorname{div}\mathbf{u}\,, \operatorname{div}\mathbf{v})\,, \tag{6}$$

$$L(\mathbf{v}) := (\mathbf{f}\,, \mathbf{v}) - \int_{\Gamma_1} \mathbf{g}^T\mathbf{v}\,\mathrm{d}s, \tag{7}$$

where $\mathbf{f} \in [L_2(\Omega)]^d$ and $\mathbf{g} \in [L_2(\Gamma_1)]^d$.

To investigate the robustness of the proposed method we will also consider one example with an orthotropic material (cf. [12, 24]). In this case Hooke's law is given by $\boldsymbol{\sigma} = C_{\text{ortho}} \cdot \boldsymbol{\varepsilon}$ where

$$C_{\text{ortho}}^{-1} := \begin{pmatrix} 1/E_1 & -\nu_{12}/E_1 & -\nu_{13}/E_1 & 0 & 0 & 0 \\ -\nu_{12}/E_1 & 1/E_2 & -\nu_{23}/E_2 & 0 & 0 & 0 \\ -\nu_{13}/E_1 & -\nu_{23}/E_2 & 1/E_3 & 0 & 0 & 0 \\ 0 & 0 & 0 & 1/\mu_{23} & 0 & 0 \\ 0 & 0 & 0 & 0 & 1/\mu_{13} & 0 \\ 0 & 0 & 0 & 0 & 0 & 1/\mu_{12} \end{pmatrix}, \tag{8}$$

E_i is the Young's modulus in the x_i-direction, μ_{ij} is the shear modulus in the x_i-x_j-plane and ν_{ij} is the major Poisson ratio. This constitutive law is determined by 9 unknowns. Hence, using (8) in (2a) yields the following bilinear form

$$a_{\text{ortho}}(\mathbf{u}, \mathbf{v}) := \int_\Omega C_{\text{ortho}} \cdot \boldsymbol{\varepsilon}(\mathbf{u}) : \boldsymbol{\varepsilon}(\mathbf{v}) \, \mathrm{d}\mathbf{x} \,. \tag{9}$$

The existence and uniqueness of our variational problem (5) for both bilinear forms, (6) and (9), follows from the Lax-Milgram-theorem together with Korn's inequality, since the stress-strain matrices C_{iso} as well as C_{ortho} are SPD for reasonable parameter settings.

In order to solve this system numerically we use finite elements. Therefore, we consider a regular triangulation $\mathcal{T}_h = \{T\}$ depending on the mesh size parameter h of the d-dimensional (here $d = 3$) domain. We use tetrahedral meshes. Furthermore, we restrict all our considerations to first-order schemes in this article. That is, we define the piecewise linear (vector-valued) continuous functions by

$$V_h := \{\mathbf{v}_h \in [C^0(\overline{\Omega})]^d \,:\, v_i|_T \in P_1(T),\, 1 \le i \le d,\, \forall T \in \mathcal{T}_h\}. \tag{10}$$

We will focus on linear systems (1) that stem from the following FE-problem, which we will refer to as linear elasticity problem.

Problem 2.1. *Find* $\mathbf{u}_h \in V_h$ *defined by* (10) *such that*

$$a(\mathbf{u}_h, \mathbf{v}_h) = L(\mathbf{v}_h) \qquad \forall \mathbf{v}_h \in V_h \,, \tag{11}$$

where the bilinear form $a(\cdot,\cdot)$ *is either given by* (6) *or by* (9) *and the linear form* $L(\cdot)$ *is defined by* (7)*.*

When employing the bilinearform $a_{\text{iso}}(\cdot,\cdot)$ and $a_{\text{ortho}}(\cdot,\cdot)$ we will call Problem 2.1 isotropic or orthotropic, respectively.

3 Approximation via edge-matrices

The AMGm method, introduced in [14] for scalar problems and extended to problems in linear elasticity in [13], is based on the construction of edge matrices, which can be used for measuring the nodal dependence. In the following we briefly describe this approach and thereby take it to a more abstract level.

We therefore introduce the terms of *algebraic vertices* and *algebraic edges*. Let $\mathcal{D} := \{d_i \,:\, i \in \{1, \ldots, n\}\}$ be the set of n degrees of freedom (DOF).

Definition 3.1 (algebraic vertex, algebraic edge and edge matrix)**.** *An* algebraic vertex $\mathbf{v}_i$ *is an accumulation of* n_{vd} *vertex degrees of freedom (VDOF), i.e.,* $\mathbf{v}_i = \{d_{i_j} \,:\, j \in \{1, \ldots, n_{vd}\}\}$*. Furthermore for any* $\mathbf{v}_i$ *and* $\mathbf{v}_j$ *with* $i \neq j$ *it holds that* $\mathbf{v}_i \cap \mathbf{v}_j = \emptyset$*. Let* $\mathcal{V}$

denote the set of all vertices and n_v its cardinality, that is $n_v = |\mathcal{V}|$.
An algebraic edge e_{ij} *is a connection of two different algebraic vertices* $\mathbf{v}_i$ *and* $\mathbf{v}_j$*;* $\mathcal{E} := \{e_{ij} : 1 \leq i < j < n_v\}$ *denotes the set of all* n_e *edges*[1].
An edge matrix E_{ij} *is an* $2n_{vd} \times 2n_{vd}$*-matrix associated with the edge* e_{ij} *which represents the relation between the algebraic vertices* $\mathbf{v}_i$ *and* $\mathbf{v}_j$[2].

Definition 3.1 is rather general and allows us to extend the following concept to different discretizations or finite elements, respectively. In our particular situation, we identify the algebraic vertices with the nodes of the mesh and assume that $n_{vd} = d$. Since we restrict ourselves to Problem 2.1 with continuous, piecewise linear shape functions this choice is quite natural.

Aligning with Defintion 3.1 we define the set of neighbors $\mathcal{N}_i$ of a vertex $\mathbf{v}_i$, that is $\mathcal{N}_i := \{\mathbf{v}_j : e_{ij} \in \mathcal{E}\}$.

Our aim is to determine the nodal dependence by means of edge matrices. For this sake we first have to investigate their desired properties. Therefore, following [13], let $\mathcal{A} = \{A_T : T \in \mathcal{T}_h\}$ bet the set of element matrices A_T corresponding to our FE-discretization of Problem 2.1 with the triangulation $\mathcal{T}_h$ of the d-dimensional domain Ω. From the coercivity of the bilinearform $a(\cdot, \cdot)$ it follows that $A_T \geq 0$, that is, A_T is symmetric positive semidefinite (SPSD). We target in approximating each single element matrix A_T by a sum of corresponding edge matrices E_{ij}. That is, we want a set of edge matrices $\mathcal{B}_T$ associated with the set of algebraic edges $\mathcal{E}_T$ of T, such that $A_T \approx B_T := \sum_{E_{ij} \in \mathcal{B}_T} E_{ij}$. Here summation has to be understood in the sense of assembling. Note that $\mathcal{B}_T$ contains only one matrix E_{ij} corresponding to each edge $e_{ij} \in \mathcal{E}_T$. This setting aligns with our general adjustment to set up one edge matrix for each algebraic edge. We want to compute an approximation B_T of A_T via a set of SPSD edge matrices $\mathcal{B}_T$ such that B_T is spectrally as close as possible to A_T. This idea has already been considered in [8]. For a more detailed discussion for systems of equations as in our case see [13].

In the following part of this section, we will characterize such approximate splittings. First, we note that an approximate splitting yields a finite condition number, i.e.

$$\kappa(A_T, B_T) := \frac{\inf\{\lambda : \mathbf{x}^T A_T \mathbf{x} \leq \lambda \mathbf{x}^T B_T \mathbf{x} \ \ \forall \mathbf{x} \in \mathbb{R}^d\}}{\sup\{\lambda : \mathbf{x}^T A_T \mathbf{x} \geq \lambda \mathbf{x}^T B_T \mathbf{x} \ \ \forall \mathbf{x} \in \mathbb{R}^d\}} < \infty\,, \tag{12}$$

if the splitting $\mathcal{B}_T$ is *kernel preserving*. In other words, for every splitting $\mathcal{B}_T$ with SPSD edge matrices $E_{ij} \in \mathcal{B}_T$, we have

$$\kappa(A_T, B_T) < \infty \ \Leftrightarrow \ \ker(B_T) = \ker(A_T) \ \Rightarrow \ \ker(E_{ij}) = \ker(A_T)|_{(ij)} \quad \forall E_{ij} \in \mathcal{B}_T \tag{13}$$

For a proof see [13]. Being aware of the necessity of kernel preservation, one can investigate the required properties of the edge matrices. In [13] the following theorem has been shown.

Theorem 3.2 (characterization of semipositive splittings)**.** *Let A_T be an SPSD element matrix arising form the (first-order) FE discretization of the 3D elasticity problem, Problem 2.1, using a (shape-regular) tetrahedral triangulation $\mathcal{T}_h$. Further, let $\mathcal{B}_T = \{E_{ij} : E_{ij} \geq 0 \ \wedge \ 1 \leq i < j \leq 4\}$ be a set of SPSD edge matrices providing the splitting $B_T = \sum_{E_{ij} \in \mathcal{B}_T} E_{ij}$.*
Then $\kappa(A_T, B_T) < \infty$ if and only if the $2n_{vd} \times 2n_{vd}$ (nonzero) edge matrices E_{ij} have the form

$$E_{ij} = c_{ij} \begin{pmatrix} \mathbf{v}_{ij}^T \mathbf{v}_{ij} & -\mathbf{v}_{ij}^T \mathbf{v}_{ij} \\ -\mathbf{v}_{ij}^T \mathbf{v}_{ij} & \mathbf{v}_{ij}^T \mathbf{v}_{ij} \end{pmatrix} \quad \textit{with} \quad \mathbf{v}_{ij} = \begin{pmatrix} x_j - x_i \\ y_j - y_i \\ z_j - z_i \end{pmatrix} \quad 1 \leq i < j \leq 4, \tag{14}$$

[1] Note that we do not distinguish between e_{ij} and e_{ji} in general since we are dealing with symmetric problems.

[2] Aligning with the convention of the edges we have $E_{ji} := E_{ij}$ for $i < j$.

and $c_{ij} > 0$. Furthermore, the vectors (x_k, y_k, z_k), $1 \leq k \leq 4$, are the vertices of the tetrahedron T.

It is obvious that the edge matrices in Theorem 3.2 are of rank one. Additionally the exact representation of each edge matrix is given by (14) which is determined up to the scalar constant c_{ij} since the vector $\mathbf{v}_{ij}$ is the directional vector of the edge e_{ij}.

As compared to the method presented in [13] we modify the construction of the edge matrices E_{ij}. This modification has several advantages, e.g., the computation of the coarse edges can be performed straightforward.

Let us consider the matrix G_h, which is assembled from all element stiffness matrices A_T of our problem. That is, we neglect all boundary terms. Hence, we have

$$A = A_h = \sum_{T \in \mathcal{T}_h} A_T + F_h =: G_h + F_h \tag{15}$$

where F_h contains the boundary terms. The matrix G_h can be represented in the form

$$G_h = \begin{bmatrix} \ddots & \vdots & \vdots & \vdots & \vdots & \vdots & \vdots \\ \dots & G_{ij} + G_{ik} + \dots & \dots & -G_{ij} & \dots & -G_{ik} & \dots \\ \vdots & \vdots & \ddots & \vdots & \vdots & \vdots & \vdots \\ \dots & -G_{ij}^T & \dots & G_{ij}^T + \dots & \dots & \dots & \dots \\ \vdots & \vdots & \vdots & \vdots & \ddots & \vdots & \vdots \\ \dots & -G_{ik}^T & \dots & \dots & \dots & G_{ik}^T + \dots & \dots \\ \vdots & \vdots & \vdots & \vdots & \vdots & \vdots & \ddots \end{bmatrix} \tag{16}$$

with $n_v \times n_v$ blocks of size $n_{vd} \times n_{vd}$. Based on the off-diagonal blocks of G_h we want to determine the contribution of the connection of the vertices $\mathbf{v}_i$ and $\mathbf{v}_j$ (algebraic edge e_{ij}). One possible choice is to use

$$\tilde{E}_{ij}^{(1)} = \begin{pmatrix} G_{ij} & -G_{ij} \\ -G_{ij}^T & G_{ij}^T \end{pmatrix}, \tag{17}$$

which is a nonsymmetric matrix in general because G_{ij} is not necessarily symmetric. On the other hand, since the diagonal blocks of G_h are symmetric $\tilde{E}_{ij}$ can also be chosen according to

$$\tilde{E}_{ij}^{(2)} = \begin{pmatrix} \frac{1}{2}(G_{ij} + G_{ij}^T) & -G_{ij} \\ -G_{ij}^T & \frac{1}{2}(G_{ij} + G_{ij}^T) \end{pmatrix}. \tag{18}$$

Note that $\tilde{E}_{ij}^{(2)}$ is symmetric. Now, we aim at approximating $\tilde{E}_{ij}^{(p)}$, $p = 1, 2$, by

$$E_{ij} := \arg\min_E \left\| E - \tilde{E}_{ij}^{(p)} \right\|^2. \tag{19}$$

Since we know the form of E_{ij} (cf. Theorem 3.2) we only have to determine c_{ij}. The solution of (19) is much easier when using the Frobenius norm instead of the l_2-norm. With this choice we arrive at

$$c_{ij} = \arg\min_c \left\| E_{ij}(c) - \tilde{E}_{ij}^{(p)} \right\|_F^2 \tag{20}$$

with

$$E_{ij}(c) = c \begin{pmatrix} \mathbf{v}_{ij}^T \mathbf{v}_{ij} & -\mathbf{v}_{ij}^T \mathbf{v}_{ij} \\ -\mathbf{v}_{ij}^T \mathbf{v}_{ij} & \mathbf{v}_{ij}^T \mathbf{v}_{ij} \end{pmatrix},$$

where $\mathbf{v}_{ij}$ is the directional vector of the edge e_{ij}.

Theorem 3.3. *Let $\tilde{E}_{ij}^{(p)}$, $p = 1, 2$, be defined by* (17) *or* (18)*. Then the minimization problem* (20) *has the solution*

$$c_{ij} = \frac{\mathbf{v}_{ij}^T G_{ij} \mathbf{v}_{ij}}{\|\mathbf{v}_{ij}\|_2^4} \,. \tag{21}$$

Proof. For simplicity we neglect the subscripts ij of the occurring vectors and matrices. From the representation of the Frobenius norm via the trace-operator we obtain

$$\|E(c) - \tilde{E}^{(p)}\|_F^2 = \operatorname{tr}(E(c)^2) + \operatorname{tr}((\tilde{E}^{(p)})^2) - 2\operatorname{tr}(E(c)\,\tilde{E}^{(p)}) \,. \tag{22}$$

Thus we have

$$\operatorname{tr}(E(c)^2) = \operatorname{tr}\left(c^2 \begin{bmatrix} 2\mathbf{v}\mathbf{v}^T\mathbf{v}\mathbf{v}^T & -2\mathbf{v}\mathbf{v}^T\mathbf{v}\mathbf{v}^T \\ -2\mathbf{v}\mathbf{v}^T\mathbf{v}\mathbf{v}^T & 2\mathbf{v}\mathbf{v}^T\mathbf{v}\mathbf{v}^T \end{bmatrix} \right) = 4c^2\|\mathbf{v}\|_2^4 \,, \tag{23}$$

and (for $p = 1$)

$$\begin{aligned} \operatorname{tr}(E(c)\,\tilde{E}^{(1)}) &= \operatorname{tr}\left(c \begin{bmatrix} \mathbf{v}\mathbf{v}^T(G+G^T) & -\mathbf{v}\mathbf{v}^T(G+G^T) \\ -\mathbf{v}\mathbf{v}^T(G+G^T) & \mathbf{v}\mathbf{v}^T(G+G^T) \end{bmatrix} \right) \\ &= 2c\operatorname{tr}(\mathbf{v}\mathbf{v}^T(G+G^T)) = 2c(\operatorname{tr}(\mathbf{v}\mathbf{v}^T G) + \operatorname{tr}(\mathbf{v}\mathbf{v}^T G^T)) \\ &= 4c\mathbf{v}^T G\mathbf{v} \,. \end{aligned} \tag{24}$$

For $p = 2$ the matrix product looks different, but its trace is identical to (24). In summary, by plugging (23) and (24) into (22) we obtain

$$\zeta(c) := \|E(c) - \tilde{E}^{(p)}\|_F^2 = 4c^2\|\mathbf{v}\|_2^4 + \operatorname{tr}((\tilde{E}^{(p)})^2) - 8c\mathbf{v}^T G\mathbf{v} \,.$$

Then, solving $\zeta'(c) = 0$ for c results in (21). Since $\zeta''(c)$ is positive, the solution is a unique minimum. □

Considering Problem 2.1 it is possible that the off-diagonal submatrices G_{ij} of the matrix G_h are indefinite and hence it might happen that (21) yields a negative c_{ij}. In this case we use the absolute value of c_{ij}. Finally, note that we get a nonnegative c_{ij} if G_{ij} is positive semidefinite which is the usual case.

4 Detection of strong couplings (nodal dependence)

In any multigrid method the error is reduced by relaxation on the one hand and by coarse-grid correction on the other hand. These two components should complement each other which means that error modes not effected by the one should be treated efficiently by the other component. In AMG one first chooses the smoother S, which is Gauss-Seidel relaxation in our case, and then constructs a coarse-grid correction that is capable of reducing algebraically smooth error modes, namely errors $\mathbf{e}$ for which

$$\|S\mathbf{e}\|_A \approx \|\mathbf{e}\|_A \tag{25}$$

holds (cf. [20]). This leads, for Gauss-Seidel-smoothers among others, to the condition that the residual $\mathbf{r} = A\mathbf{e}$ has to be small as compared to the error itself, which means that

$$(r_i =) a_{ii}e_i + \sum a_{ij}e_j \approx 0 \,. \tag{26}$$

In other words, the i-th error-component e_i is mainly determined by those e_j for which the corresponding $|a_{ij}|$ are large. In standard AMG methods (cf. [20, 6, 22]), the coarse

grid is selected based on a measure for the strength of nodal dependence. According to Reference [20] point i *strongly depends* on j if

$$-a_{ij} \geq \theta \max_{l \neq i} \{-a_{il}\},$$

with some threshold $\theta \in (0, 1]$, e.g., $\theta = 0.25$. This concept works very well for M-matrices (and for small perturbations of M-matrices), but for non-M-matrices it is not clear how to take into account positive and negative off-diagonal entries. As a remedy, proposed in [4] for finite element problems, strong connections (i, j) can be selected based on the criterion

$$\frac{|a_{ij}|}{\sqrt{a_{ii}\, a_{jj}}} \geq \theta\,. \tag{27}$$

Thereby, the entries of the local stiffness matrices A_T are used. Note that (27) measures the energy-cosine of the abstract angle between the i-th and the j-th nodal basis function. While this approach has no difficulties with non-M-matrices, it is not directly applicable in the multilevel setting since the element stiffness matrices are normally not available on all levels. Another disadvantage of measure (27) is that it is not obvious how to generalize it to vector-field problems. Considering each DOF for its own typically yields more connections than desired and might result in a lack of robustness (cf. [22, 5]).

Therefore, we propose the following approach to measure the strength of an algebraic edge e_{ij} connecting the algebraic vertices $\mathbf{v}_i$ and $\mathbf{v}_j$. We collect all edges e_{kl}, i.e., edge matrices E_{kl}, building a loop of length 3 which contains the edge e_{ij}. By assembling all these edge matrices E_{kl} we get an SPSD so-called *computational molecule* $M(i, j)$.

$$M(i, j) = E_{ij} + \sum_{k \in \mathcal{N}_i \cap \mathcal{N}_j} (E_{ik} + E_{jk}) = \begin{bmatrix} M_{ii} & M_{ij} & M_{ik} \\ M_{ji} & M_{jj} & M_{jk} \\ M_{ki} & M_{kj} & M_{kk} \end{bmatrix} \tag{28}$$

with M_{ii}, $M_{jj} \in \mathbb{R}^{n_{vd} \times n_{vd}}$ and $M_{kk} \in \mathbb{R}^{|\mathcal{N}_i \cap \mathcal{N}_j| n_{vd} \times |\mathcal{N}_i \cap \mathcal{N}_j| n_{vd}}$. Now, we consider the part corresponding to the unknowns of $\mathbf{v}_i$ and $\mathbf{v}_j$ based on which we shall measure the cosine of the angle between the subspaces related to $\mathbf{v}_i$ and $\mathbf{v}_j$, which is given by the smallest possible constant in the strengthened *Cauchy-Bunyakowski-Schwarz inequality* (CBS constant).

Definition 4.1 (strong connection via CBS constant)**.** *Let the computational molecule be defined as in* (28)*. Then the strength s_{ij} of an algebraic edge e_{ij} is defined by*

$$s_{ij} := \sqrt{1 - \inf_{\mathbf{x}} \frac{\mathbf{x}^t S_{ii} \mathbf{x}}{\mathbf{x}^t M_{ii} \mathbf{x}}}\,, \tag{29}$$

where $S_{ii} := M_{ii} - M_{ij} M_{jj}^{-1} M_{ji}$.

Note that in Definition 4.1 we implicitly assume that M_{jj} is regular. If this is not the case, the Schur complement S_{ii} is replaced by the *generalized Schur complement* introduced in [13] (Algorithm 3.9). Nevertheless, if M_{ii} and M_{jj} both are regular, the strength s_{ij} of the edge e_{ij} is independent of the order of i and j and thus s_{ij} can equivalently be computed according to

$$s_{ij} = \sqrt{1 - \inf_{\mathbf{x}} \frac{\mathbf{x}^t S_{jj} \mathbf{x}}{\mathbf{x}^t M_{jj} \mathbf{x}}}\,,$$

with the Schur complement $S_{jj} := M_{jj} - M_{ji} M_{ii}^{-1} M_{ij}$. This follows directly from the definition of the CBS constant (cf. [1]).

Now, as in (27), we say a connection between the vertices $\mathbf{v}_i$ and $\mathbf{v}_j$ is strong, $\mathbf{v}_i$ strongly depends on $\mathbf{v}_j$, or the edge e_{ij} is strong, iff

$$s_{ij} \geq \theta \,, \tag{30}$$

with $\theta \in (0, 1]$. In other words, a connection between two algebraic vertices is strong if the angle between their respective subspaces, generated by $M(i, j)$, is less than a certain threshold $\arccos(\theta)$. In the following, let $\mathcal{S}_i$ denote the set of strongly connected neighbors of a vertex $\mathbf{v}_i$, i.e., $\mathcal{S}_i := \{\mathbf{v}_j \,:\, \mathbf{v}_j \in \mathcal{N}_i \wedge s_{ij} \geq \theta\}$.

It is reasonable to choose $\theta \in (0, 1]$ in order to control the fraction $\Theta \cdot n_e$ of weak edges. Later, in the numerical examples (see Section 8) $\Theta = 0.08$ was chosen. Note that increasing the number of strong edges, i.e., decreasing Θ, typically results in a faster coarsening.

5 Coarse-grid selection

Based on the *strength of connectivity* s_{ij}, associated with the algebraic edges e_{ij}, we select our coarse grid. Following the recent articles [13, 14] the same coarsening strategy as explained in [14] is used, which is a slight modification of the coarse-grid selection procedure proposed by Ruge and Stüben in [20]. We divide our set of vertices $\mathcal{V}$ into a set of fine vertices $\mathcal{V}_f$, $n_{vf} := |\mathcal{V}_f|$, and a set of coarse vertices $\mathcal{V}_c$, $n_{vc} := |\mathcal{V}_c|$. Corresponding to this partitioning we define the set of fine neighbors $\mathcal{N}_i^f := \{\mathbf{v}_j \,:\, \mathbf{v}_j \in \mathcal{N}_i \cap \mathcal{V}_f\}$ and the set of coarse neighbors $\mathcal{N}_i^c := \{\mathbf{v}_j \,:\, \mathbf{v}_j \in \mathcal{N}_i \cap \mathcal{V}_c\}$ of a vertex $\mathbf{v}_i$. Moreover, let the sets of strongly connected fine and coarse neighbors be denoted by $\mathcal{S}_i^f := \{\mathbf{v}_j \,:\, \mathbf{v}_j \in \mathcal{S}_i \cap \mathcal{V}_f\}$ and $\mathcal{S}_i^c := \{\mathbf{v}_j \,:\, \mathbf{v}_j \in \mathcal{S}_i \cap \mathcal{V}_c\}$, respectively.

When we have selected the coarse grid, we can set up a prolongation operator P and compute the coarse grid matrix A_H via the Galerkin approach, i.e., $A_H := P^T A_h P$. In the case of a two-level method, the knowledge of A_h and P is sufficient to set up the whole procedure. However, in the multilevel setting we need edges e_{ij}^c and their corresponding matrices E_{ij}^c on the coarse level. Those can be constructed in a straightforward way.

We consider the matrix G_h (see (16)). Via the Galerkin approach we compute $G_H = P^T G_h P$. Then, if we know the coordinates of the coarse vertices we can proceed in the following way. We set up a coarse edge e_{ij} connecting the coarse vertices $\mathbf{v}_i$ and $\mathbf{v}_j$ if they are strongly connected on the fine grid via at most two edges. The respective edges can be determined via the adjacency matrix product $\mathcal{E}_c = ((\mathcal{E}_{fc}^s)^T \times \mathcal{E}_{fc}^s) \vee \mathcal{E}_{cc}$. Here $\mathcal{E}_{fc}^s$ denotes the adjacency matrix of the strong connections between fine and coarse vertices, $\mathcal{E}_{cc}$ represents the coarse-to-coarse adjacency on the fine mesh, and $\mathcal{E}_c$ is the coarse-level adjacency matrix. Alternatively, one could add coarse edges between any pair of coarse vertices $\mathbf{v}_i$ and $\mathbf{v}_j$ if there exists a *strong* path of length three between them. However, if these latter mentioned coarse edges are added the coarse-grid operators of our method typically become significantly denser.

As can be seen later (in Section 6), we will use a locally energy-minimizing interpolation that involves the inverse of a small-sized matrix M_{ff} (cf. (32)–(34)). The regularity of M_{ff} demands a proper selection of coarse vertices locally, which in practice can be achieved by enriching $\mathcal{V}_c$.

To illustrate the effect of the coarsening process let us consider Problem 2.1 on the unit square Ω in 2D. We examine the effect of varying the stress-strain matrix C and also the influence of changing the mesh.

Figure 1(a) shows the fine grid and the first four coarse grids of the actual example for an isotropic constitutive-law. Thereby a uniform mesh is used. Especially, the first two coarse levels exhibit the expected uniform coarsening in all directions. In Figure 1(b) we can see the selected grid points using some orthotropic material with a different Young's

modulus in x- and y-direction, namely $E_y/E_x = 30$. Thereby we see that coarsening proceeds faster in y-direction. On the first coarse level, many additional vertices are made coarse due to the requirement of a regular M_{ff} (sub)matrix, see (34). As Figure 1(c) shows this situation improves when using an unstructured mesh, which results in a smaller grid complexity σ^{Ω} in this example.

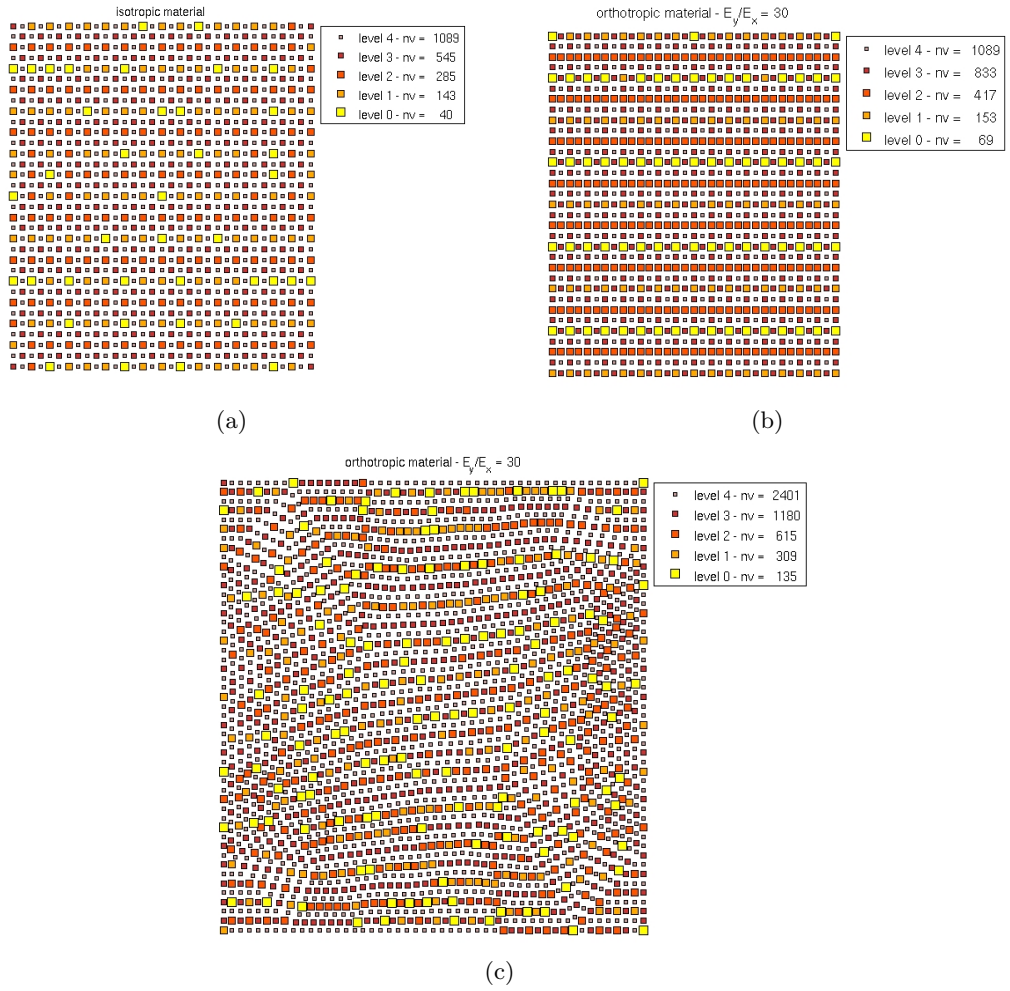

Figure 1: The coarse grid for different types of the stress-strain matrix on different meshes: isotropic material on a uniform gird (upper left); orthotropic material with $E_y/E_x = 30$ on a uniform mesh (upper right); unstructured mesh (lower picture)

6 Interpolation and smoothing

The interpolation we are using here does not differ from the one used in References [13, 14]. After reordering the vertices such that we have first the fine and then the coarse vertices, the prolongation operator $P \in \mathbb{R}^{(n_v n_{vd}) \times (n_{vc} n_{vd})}$ is given by

$$P = \begin{bmatrix} P_{\mathrm{fc}} \\ I_{\mathrm{c}} \end{bmatrix}, \tag{31}$$

where I_{c} is the identity corresponding to the coarse vertices and P_{fc} is a mapping from the $(n_{vc} n_{vd})$-dimensional coarse space onto the $(n_{vf} n_{vd})$-dimensional fine space. In order to set up the interpolation for the DOF of a fine vertex $\mathbf{v}_i$, we define the so-called interpolation

molecule

$$M(i) := \sum_{\mathbf{v}_k \in \mathcal{S}_i^c} E_{ik} + \sum_{\mathbf{v}_j \in \mathcal{S}_i^f \,:\, \exists \mathbf{v}_k \in \mathcal{S}_i^c \cap \mathcal{N}_j} E_{ij} + \sum_{\mathbf{v}_k \in \mathcal{S}_i^c, \mathbf{v}_j \in \mathcal{S}_i^f \,:\, \mathbf{v}_k \in \mathcal{S}_j^c} E_{kj} \,. \tag{32}$$

The molecule $M(i)$ emerges from the assembling of different edge matrices. The first sum in (32) comprises all edges connecting $\mathbf{v}_i$ strongly to a coarse vertex $\mathbf{v}_k$. Further, all strong fine edges e_{ij} are added if there exists a strong connection from $\mathbf{v}_j$ to one strong coarse neighbor $\mathbf{v}_k$ of $\mathbf{v}_i$. Additionally, all connections between the strong fine neighbors $\mathbf{v}_j \in \mathcal{S}_i^f$ and the strong coarse neighbors $\mathbf{v}_k \in \mathcal{S}_i^c$ are taken into account. Hence, $M(i)$ has the following block-structure

$$M(i) = \begin{bmatrix} M_{\mathrm{ff}} & M_{\mathrm{fc}} \\ M_{\mathrm{cf}} & M_{\mathrm{cc}} \end{bmatrix} . \tag{33}$$

Moreover, $M(i)$ is SPSD by construction. Following the ideas of AMGe (cf. [3, 7]) the optimal interpolation coefficients $P_{fc,i}^*$ with respect to the molecule $M(i)$ are given by

$$P_{\mathrm{fc,i}}^* := -(M_{\mathrm{ff}}^{-1} M_{\mathrm{fc}})_i \,, \tag{34}$$

where $P_{\mathrm{fc,i}}^*$ denotes the n_{vd} rows of the local interpolation matrix P_{fc} corresponding to the fine vertex $\mathbf{v}_i$. Note that this choice minimizes the following measure for the defect $\mathbf{d}_{\mathrm{f}} := \mathbf{e}_{\mathrm{f}} - P_{\mathrm{fc}}\mathbf{e}_{\mathrm{c}}$ of the local interpolation, i.e.,

$$P_{\mathrm{fc}}^* := \arg\min_{P} \max_{\mathbf{e} \perp \ker(M)} \frac{(\mathbf{e}_{\mathrm{f}} - P\mathbf{e}_{\mathrm{c}})^T (\mathbf{e}_{\mathrm{f}} - P\mathbf{e}_{\mathrm{c}})}{\mathbf{e}^T M \mathbf{e}} \,. \tag{35}$$

For further details we refer to [7, 14].

So far, we have collected all ingredients that are required to set up an AMG algorithm. As it is quite common, we use AMG to precondition the conjugate gradient (CG) method. Smoothing is performed by Gauss-Seidel, denoted by S, with a certain number of pre- and post-smoothing steps ν_1 and ν_2. Then the 2-grid algorithm reads:

Algorithm 6.1 (2-grid algorithm)**.**
$\mathbf{y} = AMG2(\mathbf{b}, \mathbf{x})$

$\tilde{\mathbf{x}} = S^{\nu_1}(\mathbf{x})$	*apply ν_1 pre-smoothing steps*
$\mathbf{d}_h = \mathbf{b} - A\tilde{\mathbf{x}}$	*compute defect*
$\mathbf{d}_H = P^T \mathbf{d}_h$	*restrict defect to coarse level*
$\mathbf{v}_H = (P^T A P)^{-1} \mathbf{d}_H$	*solve the defect equation on the coarse grid*
$\mathbf{v}_h = P\mathbf{v}_H$	*prolongate the coarse grid update to the fine level*
$\tilde{\mathbf{x}} \leftarrow \tilde{\mathbf{x}} + \mathbf{v}_h$	*update the solution*
$\mathbf{y} = S^{\nu_2}(\tilde{\mathbf{x}})$	*apply ν_2 post-smoothing steps*

Its error propagation is given by $\mathbf{e}^{(k+1)} = (I - B_{\mathrm{AMG},2}^{-1} A)\mathbf{e}^{(k)}$.

In order to set up a multilevel procedure, let us identify the components of level l with subscript (l). That is $A_{(l)} := P_{(l-1)}^T A_{(l-1)} P_{(l-1)}$ for $l = 1, \ldots, n_L$ with $A_{(0)} := A$, where n_L denotes the number of coarse levels. Additionally we introduce an integer parameter η which determines the AMG cycle. The multigrid algorithm is defined as follows.

Algorithm 6.2 (multigrid algorithm)**.**
$\mathbf{y} = AMG(\mathbf{b}, \mathbf{x}, l)$

if $l = n_L$	
$\mathbf{x} = A_{(l)}^{-1}\mathbf{b}$	*solve exactly on the coarsest level*
else	

for $s = 1 : \eta$

$\tilde{\mathbf{x}} = S^{\nu_1}(\mathbf{x})$	*apply ν_1 pre-smoothing steps*
$\mathbf{d}_{(l)} = \mathbf{b} - A_{(l)}\tilde{\mathbf{x}}$	*compute defect*
$\mathbf{d}_{(l+1)} = P_{(l)}^T \mathbf{d}_{(l)}$	*restrict defect to coarse level*
$\mathbf{v}_{(l+1)} = AMG(\mathbf{d}_{(l+1)}, \mathbf{0}, l+1)$	*solve the coarse defect equation recursively*
$\mathbf{v}_{(l)} = P_{(l)}\mathbf{v}_{(l)}$	*prolongate the coarse grid update*
$\tilde{\mathbf{x}} \leftarrow \tilde{\mathbf{x}} + \mathbf{v}_{(l)}$	*update the solution*
$\mathbf{y} = S^{\nu_2}(\tilde{\mathbf{x}})$	*apply ν_2 post-smoothing steps*

end for

end if

The choice $\eta = 1$ results in the so-called *V-cycle* while $\eta = 2$ is typically referred to as *W-cycle*.

7 Two-level convergence

In this section we will investigate the convergence properties of the two-level AMGm method, see Algorithm 6.1. As mentioned in the previous section we use AMG as a preconditioner for CG and hence the condition number of $B_{\mathrm{AMG},2}^{-1}A$, i.e., $\kappa(B_{\mathrm{AMG},2}^{-1}A)$, is the decisive measure for the convergence rate. The derivations in this section are based on the results in References [17] and [7].

First, let us assume to have a splitting of the n DOF into fine and coarse ones. Hence, we can rearrange the matrix A to obtain the following block structure

$$A = \begin{bmatrix} A_{\mathrm{ff}} & A_{\mathrm{fc}} \\ A_{\mathrm{cf}} & A_{\mathrm{cc}} \end{bmatrix}. \tag{36}$$

Using the interpolation matrix P, see (31), we compute the coarse grid matrix

$$\hat{A}_{\mathrm{c}} := P^T A P = A_{\mathrm{cc}} + A_{\mathrm{cf}}P_{\mathrm{fc}} + P_{\mathrm{fc}}^T A_{\mathrm{fc}} + P_{\mathrm{fc}}^T A_{\mathrm{ff}} P_{\mathrm{fc}}\,. \tag{37}$$

Let us study the error propagation matrix $I - B_{\mathrm{AMG},2}^{-1}A$ now. It is defined via the composition of pre-smoothing, the coarse-grid correction and post-smoothing. The iteration matrix of the coarse-grid correction step is given by

$$I - P\hat{A}_{\mathrm{c}}^{-1}P^T A \tag{38}$$

and the iteration matrix of the smoothing step is

$$S = I - M^{-1}A\,. \tag{39}$$

In order to obtain a symmetric method, the matrices for the pre- and post-smoothing steps are transposed to each other. Thence, we obtain $B_{\mathrm{AMG},2}^{-1}$ from

$$I - B_{\mathrm{AMG},2}^{-1}A = (I - M^{-1}A)(I - P\hat{A}_{\mathrm{c}}^{-1}P^T A)(I - M^{-T}A)\,. \tag{40}$$

Using the interpolation (31), we set up a basis transformation matrix

$$J = \begin{bmatrix} I & P_{\mathrm{fc}} \\ & I \end{bmatrix}. \tag{41}$$

In view of (36) the system matrix A in a hierarchical basis reads

$$\hat{A} := J^T A J = \begin{bmatrix} A_{\mathrm{ff}} & A_{\mathrm{fc}} + A_{\mathrm{ff}}P_{\mathrm{fc}} \\ A_{\mathrm{cf}} + P_{\mathrm{fc}}^T A_{\mathrm{ff}} & \hat{A}_{\mathrm{c}} \end{bmatrix}. \tag{42}$$

Note that this basis transformation leaves the ff-block unchanged, while the *cc*-block is equal to the Galerkin coarse grid matrix $\hat{A}_{\mathrm{c}}$. Furthermore, mind that the interpolation matrix P_{fc} is composed of the locally harmonic interpolation matrices (34).

Now, let us introduce the measure μ, defined by

$$\mu := \max_{\mathbf{z}\neq\mathbf{0}} \frac{(\mathbf{z}_{\mathrm{f}} - P_{\mathrm{fc}}\mathbf{z}_{\mathrm{c}})^T X_{\mathrm{ff}} (\mathbf{z}_{\mathrm{f}} - P_{\mathrm{fc}}\mathbf{z}_{\mathrm{c}})}{\mathbf{z}^T A \mathbf{z}}\,, \tag{43}$$

where X_{ff} is the ff-block corresponding to the fine-coarse partitioned matrix

$$X := M(M + M^T - A)^{-1}M^T\,, \tag{44}$$

see [17]. Note that the quantity μ is closely related to the choice of the interpolation matrix P_{fc} according to (35). Moreover, the smoothing process enters in (43) via the matrix X_{ff}. Since $A^{-1} - X^{-1} = (I - M^{-T}A)A^{-1}(I - AM^{-1})$ is SPSD it follows that $X - A \geq 0$ in a positive semidefinite sense. Reformulating (43) then yields

$$\mu = \max_{(\mathbf{d}_{\mathrm{f}}^T, \mathbf{z}_{\mathrm{c}}^T)\neq\mathbf{0}} \frac{\mathbf{d}_{\mathrm{f}}^T X_{\mathrm{ff}} \mathbf{d}_{\mathrm{f}}}{\begin{bmatrix} \mathbf{d}_{\mathrm{f}} \\ \mathbf{z}_{\mathrm{c}} \end{bmatrix}^T \hat{A} \begin{bmatrix} \mathbf{d}_{\mathrm{f}} \\ \mathbf{z}_{\mathrm{c}} \end{bmatrix}} \geq \max_{(\mathbf{d}_{\mathrm{f}}^T, \mathbf{z}_{\mathrm{c}}^T)\neq\mathbf{0}} \frac{\mathbf{d}_{\mathrm{f}}^T A_{\mathrm{ff}} \mathbf{d}_{\mathrm{f}}}{\begin{bmatrix} \mathbf{d}_{\mathrm{f}} \\ \mathbf{z}_{\mathrm{c}} \end{bmatrix}^T \hat{A} \begin{bmatrix} \mathbf{d}_{\mathrm{f}} \\ \mathbf{z}_{\mathrm{c}} \end{bmatrix}} \geq 1\,, \tag{45}$$

where $\mathbf{d}_{\mathrm{f}} = \mathbf{z}_{\mathrm{f}} - P_{\mathrm{fc}}\mathbf{z}_{\mathrm{c}}$ is the defect of the interpolation. It is usually assumed that M fulfills the so-called *smoothing property*, which implies that X is SPD (cf. [22]). For instance, Gauss-Seidel relaxation has this property.

After this short summary of the basic ingredients, we recall the following theorem, cf. [17].

Theorem 7.1 (Analysis of AMG,2)**.** *Let A be an SPD matrix partitioned in 2×2 block form (see (36)) and let P_{fc} be some interpolation matrix. Let $B_{AMG,2}$ be the AMG preconditioner defined by (40), with non-singular and symmetric smoother M such that $\|I - M^{-1}A\|_A < 1$. Let $\hat{A}$ be the matrix defined by (42), and let $\hat{\gamma}$ be the CBS constant associated with $\hat{A}$. Let X and μ be defined by (44) and (43) respectively. Then, we have*

$$\begin{aligned} \kappa(B_{AMG,2}^{-1}A) &\leq \mu \\ &\leq \frac{1}{(1-\hat{\gamma}^2)\lambda_{min}(X_{ff}^{-1}A_{ff})} \\ &\leq \frac{1}{(1-\hat{\gamma}^2)(2-\lambda_{max}(M^{-1}A))\lambda_{min}(M_{ff}^{-1}A_{ff})} \end{aligned}$$

Note that this statement is the restriction of Theorem 12 in [17] to symmetric smoothing matrices M. Additionally we have omitted the lower bounds on the condition number, since those expressions are quite involved. For instance, Jacobi relaxation yields a symmetric smoothing matrix M as well as the Gauss-Seidel method does if it is applied in a symmetric way, i.e., consecutive forward and backward smoothing.[3]

The requirement $\|I - M^{-1}A\|_A < 1$ is equivalent to the condition that the smoother S has to define a convergent iterative process. The CBS constant $\hat{\gamma}$ determines the abstract angle between the subspaces corresponding to the 2×2 partitioning of $\hat{A}$. Mind, that therein also the quality of interpolation is taken into account.

[3]The smoothing property holds for any composed relaxation process for which each component fulfills this property.

Remark. The best possible–in view of convergence–choice $P_{\rm fc} = -A_{\rm ff}^{-1}A_{\rm fc}$ results in a block-diagonal matrix $\hat{A}$ and therefore $\hat{\gamma} = 0$. However, this choice is computationally far too expensive in most practical applications.

Since in general it is difficult to determine μ, Theorem 7.1 provides further condition number bounds that involve the quality of interpolation via $\hat{\gamma}$ and spectral relations between the (sub)matrices (of) A, M and X.

In the following, we will examine the CBS constant $\hat{\gamma}$. Therefore, we will use the spectral equivalence of the element matrices A_T and the molecule matrices B_T assembled from the set $\mathcal{B}_T$ (see Section 3). That is, for each element $T \in \mathcal{T}_h$, there exist constants $\underline{c}_T$, $\overline{c}_T > 0$, such that

$$\underline{c}_T(B_T\mathbf{v}\,,\,\mathbf{v}) \le (A_T\mathbf{v}\,,\,\mathbf{v}) \le \overline{c}_T(B_T\mathbf{v}\,,\,\mathbf{v}) \qquad \forall \mathbf{v}\,. \tag{46}$$

Summing up the contributions $E_{ij,T}$ of all elements T that share a given edge e_{ij}, finally yields the edge matrix E_{ij}, i.e., $E_{ij} = \sum_{T\,:\,e_{ij}\subset T} E_{ij,T}$. Using $G = \sum_{T\in\mathcal{T}_h} A_T$ (see (15)) and $B{:=}\sum_{e_{ij}\in\mathcal{E}} E_{ij} = \sum_{T\in\mathcal{T}_h} B_T$ gives

$$\underline{c}(B\mathbf{v}\,,\,\mathbf{v}) \le (G\mathbf{v}\,,\,\mathbf{v}) \le \overline{c}(B\mathbf{v}\,,\,\mathbf{v}) \qquad \forall \mathbf{v} \tag{47}$$

with $\underline{c}{:=}\min_{T\in\mathcal{T}_h}\underline{c}_T$ and $\overline{c}{:=}\max_{T\in\mathcal{T}_h}\overline{c}_T$.

Now, let us examine the prolongation we are using according to Section 6. For simplicity in the following we assume that for interpolation of a fine vertex $\mathbf{v}_i \in \mathcal{V}_f$ the computational molecule consists of all coarse connections of vertex $\mathbf{v}_i$, i.e., $M(i){:=}\sum_{\mathbf{v}_j\in\mathcal{N}_i^c} E_{ij}$. Then the matrix B can be rewritten in the form

$$B = \sum_{\mathbf{v}_i\in\mathcal{V}_f} M(i) + \sum_{\mathbf{v}_i,\,\mathbf{v}_j\in\mathcal{V}_f\wedge e_{ij}\in\mathcal{E}} E_{ij} + \sum_{\mathbf{v}_i,\,\mathbf{v}_j\in\mathcal{V}_c\wedge e_{ij}\in\mathcal{E}} E_{ij} =: M + H\,, \tag{48}$$

where

$$M{:=}\sum_{\mathbf{v}_i\in\mathcal{V}_f} M(i) \quad\text{and}\quad H{:=}\,B - M = \begin{bmatrix} H_{\rm ff} & 0 \\ 0 & H_{\rm cc} \end{bmatrix}.$$

That is, B consists of the sum of all interpolation molecules M plus a block-diagonal remainder H. In the following we will estimate the CBS constant $\gamma(\hat{B})$ of the matrix $\hat{B}{:=}\,J^TBJ$. Since $J^TM(i)J$ is a block diagonal matrix[4] for all $\mathbf{v}_i \in \mathcal{V}_f$ it follows that $\gamma(J^TM(i)J) = 0$. Thus $\gamma(J^TMJ) = 0$, cf. Lemma 5.1 in [16]. For the examination of $\gamma(\hat{H}) = \gamma(J^THJ)$ we write $\hat{B} = J^TBJ$ in the form

$$\hat{B} = \hat{M} - c_0T + \hat{H} + c_0T$$

with $c_0 > 0$ and the block-diagonal matrix $T{:=}\,{\rm diag}(0,\,P_{\rm fc}^TH_{\rm ff}P_{\rm fc})$. If $M_{\rm cc} - c_0P_{\rm fc}^TH_{\rm ff}P_{\rm fc}$ is SPSD and does not vanish, we have $\gamma(\hat{M} - c_0T) = 0$. These requirements are fulfilled for sufficiently small $c_0 > 0$ due to the construction of $P_{\rm fc}$.
On the other hand, with J given by (41), we get

$$\bar{H}{:=}\,\hat{H} + c_0T = J^THJ + c_0T = \begin{bmatrix} H_{\rm ff} & H_{\rm ff}P_{\rm fc} \\ P_{\rm fc}^TH_{\rm ff} & H_{\rm cc} + (1+c_0)P_{\rm fc}^TH_{\rm ff}P_{\rm fc} \end{bmatrix}.$$

Since $H_{\rm ff}$ and $H_{\rm cc}$ are SPSD we have $(H_{\rm cc} + (1+c_0)P_{\rm fc}^TH_{\rm ff}P_{\rm fc})\mathbf{v}_c = 0$ for all $(\mathbf{v}_f^T,\,\mathbf{v}_c^T)^T \in \ker(\bar{H})$, which implies that $\gamma(\bar{H}) < 1$, cf. Lemma 9.1 in [1]. Now we introduce the projections $P_{\rm f}$ and $P_{\rm c}$ onto $\ker(H_{\rm ff})^\perp$ and $\ker(H_{\rm cc}+(1+c_0)P_{\rm fc}^TH_{\rm ff}P_{\rm fc})^\perp$, respectively. Since $\gamma(\bar{H}) < 1$ we can quite easily see that

$$\gamma(P_{\bar{H}}^T\bar{H}P_{\bar{H}}) = \gamma(\bar{H})\,,$$

[4]This is due to the special form of $P_{\rm fc}$, see (34).

with $P_{\bar{H}} = \mathrm{diag}(P_\mathrm{f}, P_\mathrm{c})$. Further, using $\bar{P}_\mathrm{fc} := P_\mathrm{fc} P_\mathrm{c}$ the Schur complement S_cc of $P_{\bar{H}}^T \bar{H} P_{\bar{H}}$ is given by

$$\begin{aligned} S_\mathrm{cc} &= P_\mathrm{c}^T H_\mathrm{cc} P_\mathrm{c} + (1+c_0)\bar{P}_\mathrm{fc}^T H_\mathrm{ff} \bar{P}_\mathrm{fc} - \bar{P}_\mathrm{fc}^T H_\mathrm{ff} P_\mathrm{f} (P_\mathrm{f}^T H_\mathrm{ff} P_\mathrm{f})^{-1} P_\mathrm{f}^T H_\mathrm{ff} \bar{P}_\mathrm{fc} \\ &= P_\mathrm{c}^T H_\mathrm{cc} P_\mathrm{c} + c_0 \bar{P}_\mathrm{fc}^T H_\mathrm{ff} \bar{P}_\mathrm{fc} \end{aligned}$$

because H_ff is symmetric. Thence, with $\bar{\bar{H}}_\mathrm{cc} := P_\mathrm{c}^T H_\mathrm{cc} P_\mathrm{c}$ we obtain

$$\begin{aligned} \gamma(\bar{H})^2 &= 1 - \min_{\mathbf{v}} \frac{\mathbf{v}^T S_\mathrm{cc} \mathbf{v}}{\mathbf{v}^T (P_{\bar{H}}^T \bar{H} P_{\bar{H}})_\mathrm{cc} \mathbf{v}} = 1 - \min_{\mathbf{v}} \frac{\mathbf{v}^T (\bar{\bar{H}}_\mathrm{cc} + c_0 \bar{P}_\mathrm{fc}^T H_\mathrm{ff} \bar{P}_\mathrm{fc}) \mathbf{v}}{\mathbf{v}^T (\bar{\bar{H}}_\mathrm{cc} + (1+c_0) \bar{P}_\mathrm{fc}^T H_\mathrm{ff} \bar{P}_\mathrm{fc}) \mathbf{v}} \\ &= 1 - \frac{1}{1 + \max_{\mathbf{v}} \frac{\mathbf{v}^T \bar{P}_\mathrm{fc}^T H_\mathrm{ff} \bar{P}_\mathrm{fc} \mathbf{v}}{\mathbf{v}^T (\bar{\bar{H}}_\mathrm{cc} + c_0 \bar{P}_\mathrm{fc}^T H_\mathrm{ff} \bar{P}_\mathrm{fc}) \mathbf{v}}} = 1 - \frac{1}{1 + \frac{1}{c_0 + \min_{\mathbf{v}} \frac{\mathbf{v}^T \bar{\bar{H}}_\mathrm{cc} \mathbf{v}}{\mathbf{v}^T \bar{P}_\mathrm{fc}^T H_\mathrm{ff} \bar{P}_\mathrm{fc} \mathbf{v}}}} \\ &= \frac{1}{1 + c_0 + \| \bar{\bar{H}}_\mathrm{cc}^{-1} \bar{P}_\mathrm{fc} H_\mathrm{ff} \bar{P}_\mathrm{fc} \|_2} \,. \end{aligned}$$

The previous equations hold true if $H_\mathrm{cc} \neq 0$ and $H_\mathrm{ff} \neq 0$. For $H_\mathrm{cc} \equiv 0$ we conclude $\gamma(\bar{H})^2 = \frac{1}{1+c_0}$. On the other hand, if $H_\mathrm{ff} \equiv 0$ we have $\gamma(\bar{H}) = 0$ and hence $\gamma(\hat{B}) = 0$.

Summarizing,

$$\gamma(\hat{B}) \leq \gamma(\bar{H}(c_0)) < 1 \,. \tag{49}$$

For further discussions we need the following lemma, which states the spectral equivalence of the Schur complements of spectrally equivalent matrices.

Lemma 7.2. *Let A, B be some $\mathbb{R}^{n \times n}$ matrices, $n \in \mathbb{N}$, partitioned into 2×2 blocks, see (36). Further, let A_{ff} and B_{ff} be regular and let A and B be spectrally equivalent, i.e.,*

$$\underline{c}(A\mathbf{v}\,,\,\mathbf{v}) \leq (B\mathbf{v}\,,\,\mathbf{v}) \leq \overline{c}(A\mathbf{v}\,,\,\mathbf{v}) \qquad \forall \mathbf{v} \in \mathbb{R}^n \tag{50}$$

for some $\overline{c} > \underline{c} > 0$. Then the Schur complement S_{cc}^B is spectrally equivalent to S_{cc}^A with the same constants $\underline{c}$ and $\overline{c}$.

Proof. The bounds follow from the minimization-property of the Schur complement and the spectral equivalence of A and B. For the upper bound we get

$$\begin{aligned} \mathbf{v}_\mathrm{c}^T S_\mathrm{cc}^B \mathbf{v}_\mathrm{c} &= \min_{\mathbf{v}_\mathrm{f}} \begin{bmatrix} \mathbf{v}_\mathrm{f} \\ \mathbf{v}_\mathrm{c} \end{bmatrix}^T B \begin{bmatrix} \mathbf{v}_\mathrm{f} \\ \mathbf{v}_\mathrm{c} \end{bmatrix} \\ &\leq \overline{c} \min_{\mathbf{v}_\mathrm{f}} \begin{bmatrix} \mathbf{v}_\mathrm{f} \\ \mathbf{v}_\mathrm{c} \end{bmatrix}^T A \begin{bmatrix} \mathbf{v}_\mathrm{f} \\ \mathbf{v}_\mathrm{c} \end{bmatrix} = \overline{c} \mathbf{v}_\mathrm{c}^T S_\mathrm{cc}^A \mathbf{v}_\mathrm{c} \,. \end{aligned}$$

The lower bound is obtained in an analogous manner. □

In view of the previous observations we are able to derive the following upper bound for $\gamma(\hat{G})$.

Theorem 7.3. *Let $\hat{G} = J^T G J$ and $\hat{B} = J^T B J$ be defined by (15) and (48) using (41). Further, let (47) be satisfied. Then, we get the following bound for the CBS constant $\gamma(\hat{G})$:*

$$\gamma(\hat{G}) \leq \sqrt{1 - (1 - \gamma(\bar{H})^2) \frac{\underline{c}}{\overline{c}}} \,. \tag{51}$$

Proof. First, note that (47) implies the spectral equivalence of $\hat{G}$ and $\hat{B}$ with the same constants $\underline{c}$ and $\overline{c}$. Now, let $P_\mathrm{f} : \mathbb{R}^{\dim(\ker(\hat{G}_\mathrm{ff})^\perp)} \to \ker(\hat{G}_\mathrm{ff})^\perp$ and $P_\mathrm{c} : \mathbb{R}^{\dim(\ker(\hat{G}_\mathrm{cc})^\perp)} \to$

$\ker(\hat{G}_{\rm cc})^\perp$ denote the projectors onto the orthogonal complements of the kernels of $\hat{G}_{\rm ff}$ and $\hat{G}_{\rm cc}$, respectively. Then we conclude for $\gamma(\hat{G})$

$$\begin{aligned}\gamma(\hat{G}) &= \sup_{\substack{\mathbf{v}_{\rm f}\notin\ker(\hat{G}_{\rm ff})\\ \mathbf{v}_{\rm c}\notin\ker(\hat{G}_{\rm cc})}} \frac{\mathbf{v}_{\rm f}^T\hat{G}_{\rm fc}\mathbf{v}_{\rm c}}{\sqrt{\mathbf{v}_{\rm f}^T\hat{G}_{\rm ff}\mathbf{v}_{\rm f}\cdot\mathbf{v}_{\rm c}^T\hat{G}_{\rm cc}\mathbf{v}_{\rm c}}}\\ &= \sup_{\mathbf{v}_{\rm f},\,\mathbf{v}_{\rm c}\neq\mathbf{0}} \frac{\mathbf{v}_{\rm f}^T P_{\rm f}^T\hat{G}_{\rm fc}P_{\rm c}\mathbf{v}_{\rm c}}{\sqrt{\mathbf{v}_{\rm f}^T P_{\rm f}^T\hat{G}_{\rm ff}P_{\rm f}\mathbf{v}_{\rm f}\cdot\mathbf{v}_{\rm c}^T P_{\rm c}^T\hat{G}_{\rm cc}P_{\rm c}\mathbf{v}_{\rm c}}} = \gamma(\hat{P}^T\hat{G}\hat{P})\,,\end{aligned}$$

with $\hat{P}:=\operatorname{diag}(P_{\rm f},\,P_{\rm c})$. Analogously, we get $\gamma(\hat{B})=\gamma(\hat{P}^T\hat{B}\hat{P})$. Now, we obtain with Lemma 7.2 (using also Lemma 9.2 in [1])

$$\begin{aligned}1-\gamma(\hat{G})^2 &= 1-\gamma(\hat{P}^T\hat{G}\hat{P})^2 = \inf_{\mathbf{v}_{\rm c}\neq\mathbf{0}}\frac{\mathbf{v}_c^T S_{\rm cc}^{\hat{P}^T\hat{G}\hat{P}}\mathbf{v}_c}{\mathbf{v}_{\rm c}P_{\rm c}^T\hat{G}_{\rm cc}P_{\rm c}\mathbf{v}_{\rm c}}\\ &\geq \frac{\underline{c}}{\overline{c}}\inf_{\mathbf{v}_{\rm c}\neq\mathbf{0}}\frac{\mathbf{v}_c^T S_{\rm cc}^{\hat{P}^T\hat{B}\hat{P}}\mathbf{v}_c}{\mathbf{v}_{\rm c}P_{\rm c}^T\hat{B}_{\rm cc}P_{\rm c}\mathbf{v}_{\rm c}} = \frac{\underline{c}}{\overline{c}}(1-\gamma(\hat{P}^T\hat{B}\hat{P})^2) = \frac{\underline{c}}{\overline{c}}(1-\gamma(\hat{B})^2)\\ &\geq (1-\gamma(\bar{H})^2)\frac{\underline{c}}{\overline{c}}\,,\end{aligned}$$

from which (51) follows. □

Remark. So far we have investigated the CBS constant of $\hat{G}=J^TGJ$, where G is defined by (15). From $\hat{A}=\hat{G}+\hat{F}$ we conclude that

$$\gamma(\hat{A})\leq\max\{\gamma(\hat{G}),\,\gamma(\hat{F})\}\,.$$

Hence, assuming that $\gamma(\hat{F})\leq\gamma(\hat{G})$ we obtain with (51)

$$\gamma(\hat{A})\leq\sqrt{1-(1-\gamma(\bar{H})^2)\frac{\underline{c}}{\overline{c}}}\,. \tag{52}$$

In the remainder of this section we study by means of an example the spectral equivalence of A_T and B_T, i.e., the evaluation of $\gamma(\hat{G})$.

We have seen in Theorem 3.2 that the edge matrices E_{ij} are of the form (14), that is, only c_{ij} is left to be determined. Therefore, we investigate the minimal relative condition number $\kappa(A_T,\,B_T)$ for the reference element, see Figure 2. In the two-dimensional case we compare the best possible $\kappa(A_T,\,B_T)$,[5] depicted by the solid line, to the relative condition number that is obtained when choosing c_{ij} according to (21). The latter curve is dotted. We see that using (21) yields a condition number which is quite close to the optimal. Additionally to the condition numbers in 2D, the dashed line in Figure 2 describes $\kappa(A_T,\,B_T)$ obtained for the reference tetrahedron in 3D. For reasonable ν we still get acceptable results. Furthermore we observe the large slope of κ when ν approaches to 1/2. This is due to the ill-posedness of the system (2) in the limit case $\nu=1/2$. For instance, we have $\kappa(A_T,\,B_T)=11.2$ (22.6) for $\nu=0.45$ in 2D (3D).

8 Numerical results

In the following we discuss the numerical results obtained by applying the AMGm method to selected linear elasticity problems. We consider three different examples. The first one is a composite material consisting of two different matters which differ in their Young's

[5] The best possible κ was computed by minimizing $\kappa(A_T,\,B_T)$ with respect to the c_{ij}.

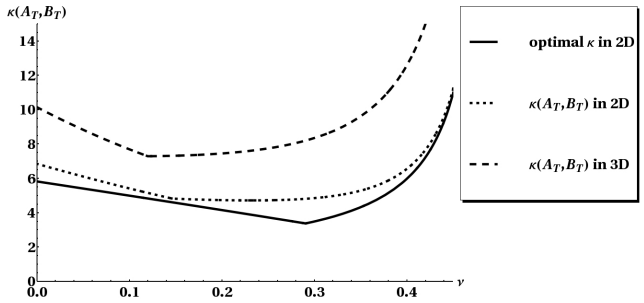

Figure 2: The general condition numbers $\kappa(A_T, B_T)$ for optimal constants c_{ij} (solid line) and for the constants according to AMGm in 2D (dotted line) and 3D (dashed line).

modulus. The second example is a beam with a locally refined grid. In the last part of this section we are dealing with orthotropic materials, such as wood and cancellous bones.

AMGm has been implemented as a preconditioner for the preconditioned conjugate gradient method in the finite element software package NGSolve (see [21]). As a smoother we use a symmetric block Gauss-Seidel method. We perform tests with the V- and with the W-cycle AMGm preconditioner with one pre- and one post-smoothing step, denoted by V(1,1) and W(1,1). For these settings the number of iterations (#it) and the average convergence factor (ρ) are listed for a reduction of the initial residual by a factor of 10^8. The numbers in the tables are the results obtained when using the auxiliary matrix G for the computation of the edge matrices, while the numbers in parenthesis refer to edge-matrices that are computed directly from A instead of G on all levels. Furthermore, we report the grid and operator complexity σ^Ω and σ^A.[6] All the computations are performed on three different meshes; The two finer meshes have been generated from the coarsest mesh by uniform refinement. Finally, we mention that we use a fraction $\Theta = 0.08$ of weak edges (cf. Section 4) in all computations.

8.1 Composite Material

In this example we are dealing with a composite material. Therefore, let Ω be the unit cube, i.e., $\Omega = (0, 1)^3$, where the material is distributed checkered, as depicted in Figure 3(a). We solve Problem 2.1 where the same Poisson ratio ν, but different moduli of elasticity E, referred to as E_0 and E_1, are used. Note that only the ratio E_1/E_0 is of importance.

We fix the displacement $\mathbf{u} = 0$ at the bottom, i.e., $\Gamma_0 := [0, 1] \times [0, 1] \times \{0\}$. Further, we apply a force in the negative z-direction on the top, i.e., $\Gamma_{1,1} := [0, 1] \times [0, 1] \times \{1\}$ and impose homogeneous Neumann-boundary conditions on the remaining part of the boundary $\Gamma_{1,0} := \partial\Omega \backslash (\Gamma_0 \cup \Gamma_{1,1})$, which results in

$$\mathbf{g} = \begin{cases} \mathbf{0} & \text{on } \Gamma_{1,0} \\ (0, 0, -g_z)^T & \text{on } \Gamma_{1,1} \end{cases} . \tag{53}$$

The computations are performed for varying ratio E_1/E_0, ranging from 1 to 1 000, on three different meshes. Additionally, we have chosen two values for the Poisson ratio ν, namely $\nu = 0.2$ and $\nu = 0.4$. In Figure 3(b) the solution for $\nu = 0.2$ and $E_1/E_0 = 10$ is illustrated.

In Table 1 and Table 2 the convergence properties and complexities of the method are reported for $\nu = 0.2$ and $\nu = 0.4$, respectively. Firstly, we observe that the W-cycle

[6] σ^Ω denotes the ratio of the total number of vertices (nodes) on all levels and the number of vertices on the finest grid; σ^A, on the other hand, is the total number of nonzeros in the matrices (on all levels) divided by the number of nonzeros in the fine-grid matrix.

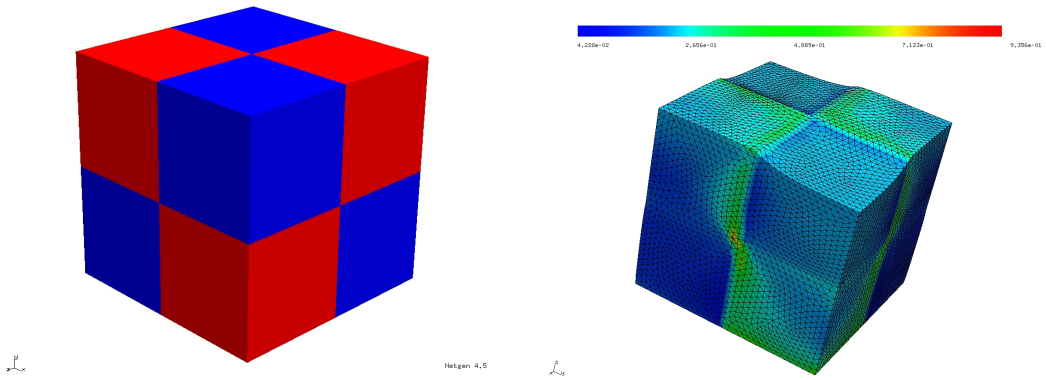

(a) geometry (b) solution for $E_1/E_0 = 10$ and $nu = 0.2$

Figure 3: Geometry and solution for the composed cube.

AMGm preconditioner results in convergence rates that are independent of the mesh size h. The operator complexity σ^A is also almost constant. For the V-cycle method, we observe a dependence of the iteration count on the mesh size h, i.e., on the number of levels n_L. Under weak assumptions the general condition number for the V-cycle preconditioner typically depends on the number of levels n_L, see, e.g., [23].[7] For a detailed discussion we refer to [23]. The second important result is the robustness with respect to the ratio E_1/E_0. Throughout both tables we can clearly see that this quotient has almost no influence on the convergence of the method. Thirdly, when comparing Table 1 to Table 2 we observe a moderate increase of the number of iterations for $\nu = 0.4$. This is due to the deterioration of $\kappa(A_T, B_T)$ defined by (12) which can be seen in Figure 2.

Table 1: Comparison of $V(1,1)$ and $W(1,1)$-cycle of PCG for $\varepsilon = 10^{-8}$ and $\nu = 0.2$ applied to a composite material.

#elements (#DOF)		22 043 (14 028)		176 344 (99 639)		1 410 752 (750 135)	
#levels		4		6		8	
$\nu = 0.2$		#it.	ρ	#it.	ρ	#it.	ρ
$E_1/E_0 = 1$:	V(1,1)	38 (28)	0.61 (0.51)	56 (42)	0.72 (0.64)	68 (50)	0.76 (0.69)
	W(1,1)	18 (13)	0.33 (0.24)	21 (13)	0.40 (0.24)	19 (14)	0.36 (0.24)
σ^Ω		1.56 (1.59)		1.50 (1.50)		1.48 (1.48)	
σ^A		3.38 (3.49)		3.41 (3.45)		3.58 (3.56)	
$E_1/E_0 = 10$:	V(1,1)	44 (39)	0.65 (0.62)	66 (59)	0.76 (0.73)	88 (60)	0.81 (0.73)
	W(1,1)	20 (17)	0.37 (0.31)	20 (17)	0.40 (0.31)	18 (14)	0.34 (0.25)
σ^Ω		1.57 (1.56)		1.50 (1.50)		1.48 (1.48)	
σ^A		3.41 (3.31)		3.38 (3.44)		3.58 (3.57)	
$E_1/E_0 = 100$:	V(1,1)	51 (39)	0.70 (0.62)	71 (70)	0.77 (0.76)	77 (73)	0.79 (0.78)
	W(1,1)	19 (15)	0.38 (0.27)	19 (17)	0.36 (0.33)	17 (14)	0.32 (0.25)
σ^Ω		1.56 (1.56)		1.50 (1.50)		1.48 (1.48)	
σ^A		3.33 (3.34)		3.44 (3.43)		3.58 (3.57)	
$E_1/E_0 = 1\,000$:	V(1,1)	42 (36)	0.64 (0.60)	78 (75)	0.79 (0.78)	79 (84)	0.79 (0.80)
	W(1,1)	16 (14)	0.31 (0.25)	19 (18)	0.36 (0.35)	15 (15)	0.28 (0.27)
σ^Ω		1.58 (1.57)		1.50 (1.50)		1.48 (1.48)	
σ^A		3.45 (3.38)		3.40 (3.43)		3.58 (3.58)	

[7] Only under a stronger "smoothing property" an h- and n_L-independent convergence rate can be proven.

Table 2: Comparison of $V(1,1)$ and $W(1,1)$-cycle of PCG for $\varepsilon = 10^{-8}$ and $\nu = 0.4$ applied to a composite material.

#elements (#DOF)		22 043 (14 028)		176 344 (99 639)		1 410 752 (750 135)	
#levels		4		6		8	
$\nu = 0.4$		#it.	ρ	#it.	ρ	#it.	ρ
$E_1/E_0 = 1$:	V(1,1)	46 (33)	0.67 (0.57)	63 (53)	0.74 (0.70)	73 (61)	0.78 (0.74)
	W(1,1)	22 (16)	0.42 (0.31)	23 (17)	0.44 (0.33)	22 (16)	0.42 (0.31)
σ^Ω		1.56 (1.58)		1.51 (1.51)		1.48 (1.48)	
σ^A		3.35 (3.45)		3.45 (3.43)		3.49 (3.49)	
$E_1/E_0 = 10$:	V(1,1)	52 (44)	0.70 (0.65)	83 (56)	0.80 (0.71)	78 (68)	0.79 (0.76)
	W(1,1)	23 (20)	0.45 (0.38)	25 (16)	0.47 (0.30)	20 (17)	0.39 (0.32)
σ^Ω		1.56 (1.57)		1.50 (1.50)		1.48 (1.48)	
σ^A		3.34 (3.44)		3.42 (3.41)		3.51 (3.49)	
$E_1/E_0 = 100$:	V(1,1)	58 (50)	0.73 (0.69)	81 (68)	0.79 (0.76)	97 (86)	0.83 (0.81)
	W(1,1)	23 (20)	0.43 (0.39)	22 (17)	0.42 (0.34)	19 (16)	0.36 (0.31)
σ^Ω		1.56 (1.57)		1.51 (1.51)		1.48 (1.48)	
σ^A		3.37 (3.41)		3.45 (3.44)		3.50 (3.49)	
$E_1/E_0 = 1000$:	V(1,1)	45 (40)	0.66 (0.63)	84 (55)	0.80 (0.71)	110 (97)	0.84 (0.83)
	W(1,1)	18 (15)	0.35 (0.29)	21 (15)	0.40 (0.28)	19 (17)	0.38 (0.30)
σ^Ω		1.56 (1.57)		1.51 (1.51)		1.48 (1.48)	
σ^A		3.34 (3.41)		3.47 (3.47)		3.51 (3.49)	

8.2 Beam

Now, we investigate the influence of the shape of the reference configuration by means of a beam, i.e., $\Omega = (0,\, 20) \times (0,\, 2) \times (0,\, 1)$ consisting of an isotropic material ($C = C_{\text{iso}}$ defined by (3)). We fix the deformation on both ends of the beam to be zero, that is,

$$\mathbf{u} = \mathbf{0} \qquad \text{on } \Gamma_0 := \{0,\, 20\} \times [0,\, 2] \times [0,\, 1]\,.$$

Moreover, we apply some force in negative z-direction on a circle $\Gamma_{1,1} := \{\mathbf{x} : (x_1 - 10)^2 + (x_2 - 1)^2 \leq 0.25 \wedge x_3 = 1\}$. On the remaining part of the boundary $\Gamma_{1,0} := \partial\Omega \backslash \{\Gamma_0 \cup \Gamma_{1,1}\}$ we impose homogenous Neumann boundary conditions. Hence $\mathbf{g}$ is given by (53) for some $g_z > 0$.

In Figure 4 the solution of the system (2) on the second finest mesh is shown. The shading represents the absolute value of the stress. One can see the local refinement of the mesh around $\Gamma_{1,1}$. We report the convergence history of AMGm in Table 3 for $\nu = 0.1,\, 0.25,\, 0.4$ on three different meshes, which are obtained by uniform refinement of the coarsest mesh.

We discover again a uniform convergence with respect to the mesh size when dealing with the W-cycle and an n_L- or h-dependence of the V-cycle method. Moreover, we also see a slight diminishment of the performance for increasing ν, for which the approximation B_T of A_T suffers. Another interesting observation is the rise in the operator complexity σ^A for finer meshes, the reason for which is that on coarser levels less interpolants are available for each fine vertex due to the thin-body geometry. That is, on levels with a small number of algebraic vertices we observe fewer strong connections and hence the nonzeros in the matrices $A_{(l)}$ for large l and small numbers of algebraic vertices are less than usual. Contrary, we observe a similar coarsening ratio as for standard geometries, like a cube, on the finer levels.

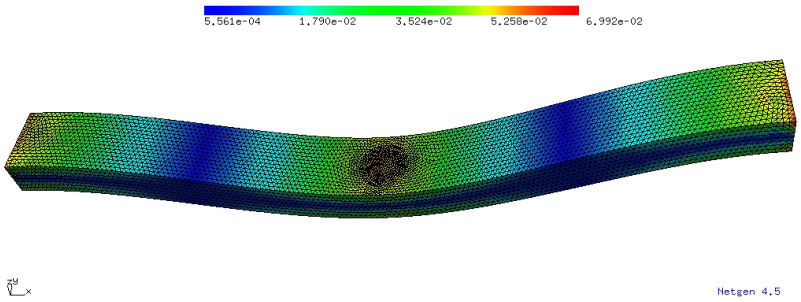

Figure 4: The deformed beam.

Table 3: Comparison of $V(1,1)$- and $W(1,1)$-cycle of PCG for $\varepsilon = 10^{-8}$ for the 3D beam.

# elements (#DOF)		22 008 (14 493)		176 064 (101 379)		1 408 512 (756 435)	
#levels		4		6		8	
		#it.	ρ	#it.	ρ	#it.	ρ
$\nu = 0.10$:	V(1,1)	59 (47)	0.73 (0.67)	99 (78)	0.83 (0.79)	128 (95)	0.87 (0.82)
	W(1,1)	24 (17)	0.45 (0.32)	28 (19)	0.51 (0.36)	25 (16)	0.46 (0.31)
σ^Ω		1.54 (1.56)		1.51 (1.51)		1.49 (1.49)	
σ^A		2.65 (2.73)		3.11 (3.13)		3.43 (3.44)	
$\nu = 0.25$:	V(1,1)	58 (41)	0.72 (0.63)	103 (57)	0.83 (0.72)	142 (84)	0.88 (0.80)
	W(1,1)	26 (16)	0.48 (0.31)	27 (15)	0.50 (0.27)	25 (15)	0.48 (0.28)
σ^Ω		1.54 (1.54)		1.50 (1.51)		1.49 (1.49)	
σ^A		2.66 (2.66)		3.05 (3.09)		3.37 (3.37)	
$\nu = 0.4$:	V(1,1)	71 (40)	0.77 (0.63)	116 (77)	0.85 (0.79)	125 (104)	0.86 (0.84)
	W(1,1)	29 (18)	0.52 (0.34)	33 (20)	0.56 (0.38)	28 (18)	0.51 (0.35)
σ^Ω		1.53 (1.54)		1.50 (1.50)		1.48 (1.48)	
σ^A		2.64 (2.69)		3.03 (3.01)		3.30 (3.29)	

8.3 Orthotropic Materials

In our last example we treat orthotropic materials with $C = C_{\text{ortho}}$ defined by (8). We will consider system (2) for three different materials, which are cancellous bone, hard and soft wood. The parameter settings for these materials are taken from [24] and for the cancellous bone additionally from [11]. As in Subsection 8.1 we consider again a cube $\Omega := (0, 1)^3$ with no displacement on the bottom $\Gamma_0 := [0, 1]^2 \times \{0\}$ and some applied force on the top $\Gamma_{1,1} := [0, 1]^2 \times \{1\}$. Moreover, we have homogeneous Neumann-boundary conditions on the remaining part of the boundary $\Gamma_{1,0} := \partial\Omega \backslash (\Gamma_0 \cup \Gamma_{1,1})$, which yields

$$\mathbf{g} = \begin{cases} \mathbf{0} & \text{on } \Gamma_{1,0} \\ g \cdot (1,\, 1,\, -1)^T & \text{on } \Gamma_{1,1} \end{cases},$$

with $g > 0$. In Table 4 we list the parameters for C_{ortho} as given in [24]. Thereby ϕ denotes the volume fraction of the cancellous bone, that is, the ratio between the volume of the solid phase of the bone and its total volume. Additionally, we identify E_t with the isotropic tissue modulus. We choose $E_t = 5.4\,\text{GPa}$ throughout all computations, which is an average value of different types of bones (cf. [11]). According to [24], the apparent density ρ of wood is related to ϕ via $\rho = \gamma\,\phi$ with $\gamma \approx 1.9\,\text{g/cm}^3$.

In the following we will examine the degree of anisotropy ω, which we define as the maximum ratio of the Youngs's moduli, that is, $\omega := \max_{i \neq j \in \{1,2,3\}} E_i/E_j$. In Figure 5(a) ω is depicted for varying volume fraction ϕ. For soft wood we find an increase of the

Table 4: Parameters for the stress-strain matrix C_{ortho} for three different materials.

	cancellous bone	hard wood	soft wood
E_1	$1\,240\,E_t\,\phi^{1.80}$	$1.307\,\rho^{0.89}$ GPa	$2.05\,\rho^{1.71}$ GPa
E_2	$885\,E_t\,\phi^{1.89}$	$2.97\,\rho^{1.50}$ GPa	$3.14\,\rho^{1.59}$ GPa
E_3	$528.8\,E_t\,\phi^{1.92}$	$27.63\,\rho^{1.41}$ GPa	$32.01\,\rho^{1.01}$ GPa
μ_{12}	$486.3\,E_t\,\phi^{1.98}$	$0.4125\,\rho^{1.21}$ GPa	$0.083\,\rho^{0.66}$ GPa
μ_{13}	$316.65\,E_t\,\phi^{1.97}$	$1.57\,\rho^{1.37}$ GPa	$2.05\,\rho^{1.36}$ GPa
μ_{23}	$266.65\,E_t\,\phi^{2.04}$	$1.97\,\rho^{1.23}$ GPa	$2.28\,\rho^{1.27}$ GPa
ν_{12}	$0.176\,E_t\,\phi^{-0.25}$	$0.724\,\rho^{0.90}$	$0.269\,\rho^{-0.17}$
ν_{13}	$0.316\,E_t\,\phi^{-0.19}$	$0.016\,\rho^{-0.76}$	$0.019\,\rho^{0.10}$
ν_{23}	$0.256\,E_t\,\phi^{-0.09}$	$0.024\,\rho^{-0.73}$	$0.028\,\rho^{0.18}$

anisotropy for decreasing ϕ. For $\phi \to 0$ the degree of anisotropy ω converges to infinity for all materials due to different exponents of ϕ and ρ in the expressions for E_i, see Table 4. For comparison, in Figure 5(b) the relative condition number $\kappa(A_T,\, B_T)$ on the reference element is plotted against ϕ. Note that the experimental data, used in [24] to derive the model (see Table 4), was available only for $\phi \in (0.05,\, 0.40)$.

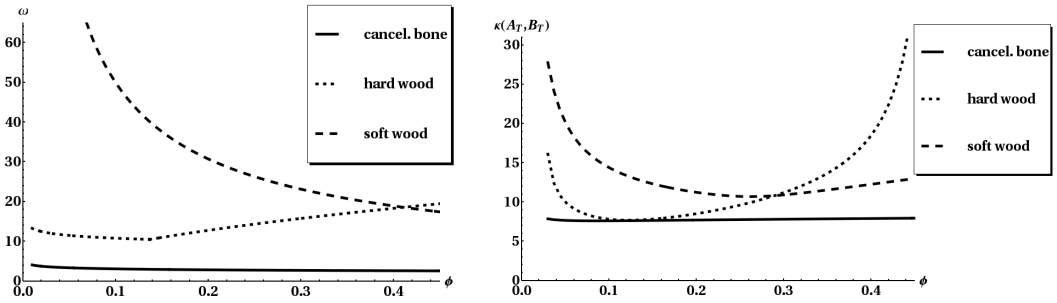

(a) the anisotropy ω (b) the relative condition number $\kappa(A_T,\, B_T)$

Figure 5: Anisotropy and the relative condition number for the 3 materials and varying ϕ.

For the numerical tests, we use two values of ϕ, i.e., $\phi = 0.3$ and $\phi = 0.1$. The corresponding values of C_{ortho} are listed in Table 5. The solution of Problem 2.1 for $\phi = 0.1$ on a mesh of approximately 33 000 vertices is shown in Figure 6. We choose $g = 2\,\text{kN}$ for a cube with a side length of 1 cm. One can clearly see a stronger deformation of the hard wood, while the cancellous bone does almost not deform due to the higher Young's moduli E_i.

Finally, in Table 6 and Table 7 the computational results are listed. First we note the stable operator complexity σ^A. Furthermore we observe uniform convergence with respect to the mesh size h and the number of levels n_L for all considered materials when employing the $W(1,1)$-cycle preconditioner. The iteration counts and the convergence factors are reflected in the relative condition numbers of the edge-matrix approximations, see Figure 5(b). For the cancellous bone the number of iterations slightly increases when changing ϕ from 0.3 to 0.1. On the other hand, the convergence in the latter case is even faster for hard wood. Soft wood shows similar properties in both settings.

Acknowledgments. The authors gratefully acknowledge the support by the Austrian Academy of Sciences and by the Austrian Science Foundation (FWF). The first author has been supported by the FWF (Project No. P19170-N18).

Table 5: Parameters for the stress-strain matrix C_{ortho} for three different materials. The moduli E_i and G_{ij} are given in GPa. $E_t = 5.4\,\text{GPa}$ and $\rho = \gamma\,\phi$ with $\gamma = 1.9\text{g/cm}^3$ (constant) were chosen.

	$\phi = 0.3$			$\phi = 0.1$		
	cancel. bone	hard wood	soft wood	cancel. bone	hard wood	soft wood
E_1	766.7	0.793	0.784	106.1	0.298	0.120
E_2	491.0	1.278	1.285	61.57	0.246	0.224
E_3	283.0	12.51	18.14	34.33	2.657	5.982
μ_{12}	242.1	0.209	0.057	27.50	0.055	0.028
μ_{13}	159.6	0.727	0.954	18.32	0.161	0.214
μ_{23}	123.5	0.987	1.117	13.13	0.255	0.277
ν_{12}	0.238	0.437	0.296	0.313	0.162	0.357
ν_{13}	0.397	0.025	0.018	0.489	0.057	0.016
ν_{23}	0.285	0.036	0.025	0.315	0.081	0.021

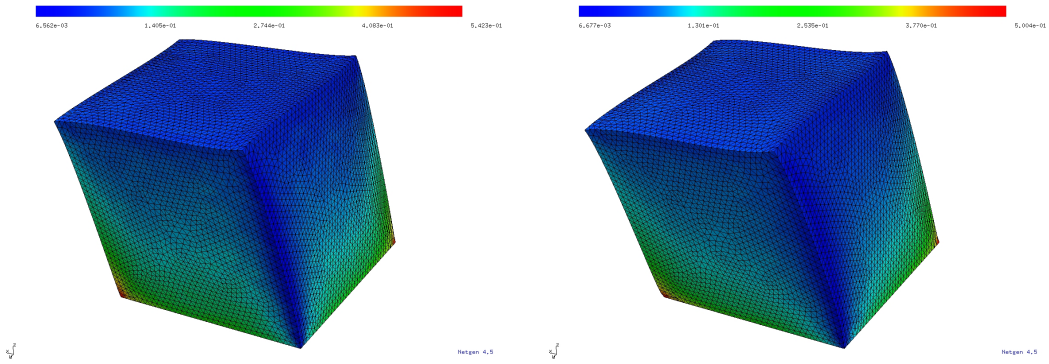

(a) soft wood

(b) hard wood

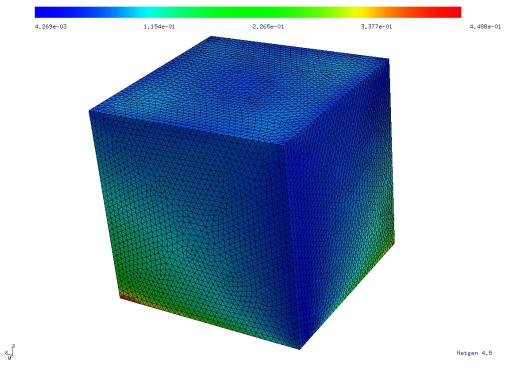

(c) cancellous bone

Figure 6: The deformed cube using the stress-strain matrix of different orthotropic materials. The color corresponds to the absolute value of the stress.

Table 6: Comparison of $V(1,1)$- and $W(1,1)$-cycle of PCG for $\varepsilon = 10^{-8}$ for the different orthotropic materials and a volume fraction $\phi = 0.3$.

#elements (#DOF)		21 473 (13 992)		171 784 (98 259)		1 374 272 (735 303)	
#levels		4		6		8	
		#it.	ρ	#it.	ρ	#it.	ρ
bone:	V(1,1)	34 (32)	0.58 (0.56)	49 (51)	0.68 (0.69)	57 (58)	0.72 (0.73)
	W(1,1)	16 (14)	0.30 (0.24)	16 (15)	0.30 (0.27)	14 (13)	0.26 (0.22)
σ^Ω		1.58 (1.58)		1.51 (1.51)		1.48 (1.48)	
σ^A		3.41 (3.49)		3.42 (3.42)		3.39 (3.39)	
hard wood:	V(1,1)	42 (35)	0.64 (0.59)	65 (61)	0.75 (0.74)	78 (67)	0.79 (0.76)
	W(1,1)	19 (15)	0.36 (0.29)	24 (20)	0.45 (0.40)	21 (18)	0.41 (0.34)
σ^Ω		1.59 (1.58)		1.51 (1.51)		1.48 (1.49)	
σ^A		3.54 (3.42)		3.46 (3.44)		3.47 (3.47)	
soft wood:	V(1,1)	51 (44)	0.69 (0.65)	81 (75)	0.79 (0.78)	100 (86)	0.83 (0.81)
	W(1,1)	24 (22)	0.46 (0.41)	30 (29)	0.53 (0.52)	29 (27)	0.53 (0.50)
σ^Ω		1.60 (1.59)		1.52 (1.52)		1.49 (1.49)	
σ^A		3.57 (3.51)		3.58 (3.54)		3.57 (3.58)	

Table 7: Comparison of $V(1,1)$- and $W(1,1)$-cycle of PCG for $\varepsilon = 10^{-8}$ for the different orthotropic materials and a volume fraction $\phi = 0.1$.

#elements (#DOF)		21 473 (13 992)		171 784 (98 259)		1 374 272 (735 303)	
#levels		4		6		8	
		#it.	ρ	#it.	ρ	#it.	ρ
bone:	V(1,1)	37 (34)	0.61 (0.57)	58 (51)	0.73 (0.70)	71 (61)	0.77 (0.74)
	W(1,1)	17 (15)	0.34 (0.28)	20 (16)	0.37 (0.32)	19 (15)	0.36 (0.28)
σ^Ω		1.59 (1.58)		1.51 (1.51)		1.48 (1.48)	
σ^A		3.59 (3.41)		3.44 (3.41)		3.37 (3.38)	
hard wood:	V(1,1)	41 (34)	0.63 (0.58)	63 (54)	0.74 (0.71)	79 (63)	0.79 (0.74)
	W(1,1)	18 (16)	0.36 (0.30)	23 (18)	0.45 (0.36)	22 (17)	0.43 (0.33)
σ^Ω		1.58 (1.59)		1.51 (1.52)		1.49 (1.49)	
σ^A		3.39 (3.48)		3.51 (3.53)		3.53 (3.53)	
soft wood:	V(1,1)	46 (44)	0.67 (0.66)	83 (76)	0.80 (0.78)	103 (80)	0.84 (0.79)
	W(1,1)	21 (21)	0.40 (0.40)	30 (26)	0.53 (0.49)	26 (25)	0.49 (0.47)
σ^Ω		1.59 (1.59)		1.52 (1.52)		1.50 (1.50)	
σ^A		3.46 (3.49)		3.60 (3.57)		3.63 (3.61)	

References

[1] O. Axelsson. *Iterative Solution Methods*. Cambridge University Press, 1994.

[2] D. Braess. *Finite Elements: Theory, Fast Solvers and Applications in Solid Mechanics*. Cambridge University Press, 2001.

[3] M. Brezina, A. J. Cleary, R. D. Falgout, V. E. Henson, J. E. Jones, T. A. Manteuffel, S. F. McCormick, and J. W. Ruge. Algebraic multigrid based on element interpolation (amge). *SIAM J. Sci. Comput.*, 22(5):1570–1592, 2001.

[4] T. F. Chan and P. Vanek. Detection of strong coupling in algebraic multigrid solvers. In *Multigrid Methods VI*, pages 11–23. Springer-Verlag, 2000.

[5] Edmond Chow. An unstructured multigrid method based on geometric smoothness. *American Journal of Mathematics*, 65:197–215, 2001.

[6] Andrew J. Cleary, Robert D. Falgout, Van Emden Henson, Jim E Jones, Thomas A. Manteuffel, Stephen F. Mccormick, Gerald N Miranda, and John Ruge. Robustness and scalability of algebraic multigrid. *SIAM J. Sci. Comput*, 21:1886–1908, 1998.

[7] R. D. Falgout and P. S. Vassilevski. On generalizing the algebraic multigrid framework. *SIAM Journal on Numerical Analysis*, 42(4):1669–1693, 2004.

[8] G. Haase, U. Langer, S. Reitzinger, and J. Schöberl. Algebraic multigrid methods based on element proconditioning. *Int. J. comp. Math.*, 78(4):575–598, 2001.

[9] V. E. Henson and P. Vassilevski. Element-free amge: General algorithms for computing interpolation weights in amg. *SIAM J. Sci. Comput.*, 23:629–650, 2001.

[10] J. E. Jones and P. S. Vassilevski. Amge based on element agglomeration. *SIAM J. Sci. Comput.*, 23:109–133, 2001.

[11] J. Kabel, B. van Rietbergen, M. Dalstra, A. Odgaard, and R. Huiskes. The role of an effective isotropic tissue modulus in the elastic properties of cancellous bone. *Journal of Biomechanics*, 32:673–680, 1999.

[12] N. Kikuchi. *Finite Element Method in Mechanics*. Cambridge University Press, 1986.

[13] J. K. Kraus. Algebraic multigrid based on computational molecules, 2: Linear elasticity problems. *SIAM J. Sci. Comput.*, 30(1):505–524, 2008.

[14] J. K. Kraus and J. Schicho. Algebraic multigrid based on computational molecules, 1: Scalar elliptic problems. *Computing*, 77:57–75, 2006.

[15] U. Langer and J. Schicho S. Reitzinger. Symbolic methods for the element preconditioning technique. In *Proc. SNSC Hagenberg, U. Langer and F. Winkler, eds.* Springer, 2000.

[16] R.D. Lazarov and S.D. Margenov. CBS constants for multilevel splitting of graph-laplacian and application to preconditioning of discontinuous galerkin systems. *Journal of Complexity*, 42(4-6):498–515, 2007.

[17] Y. Notay. Algebraic multigrid and algebraic multilevel methods: a theoretical comparison. *Numerical Linear Algebra with Applications*, 12(5-6):419–451, 2005.

[18] J. Mandel P. Vaněk and M. Brezina. Algebraic multigrid based on smoothed aggregation for second and fourth order problems. *Computing*, 56:179–196, 1996.

[19] M. Brezina P. Vaněk and J. Mandel. Convergence of algebraic multigrid based on smoothed aggregation. *Numer. Math.*, 88:559–579, 2001.

[20] J. W. Ruge and K. Stüben. Algebraic multigrid (AMG). In S. F. McCormick, editor, *Multigrid Methods*, volume 3 of *Frontiers Appl. Math.*, pages 73–130, Philadelphia, 1987. SIAM.

[21] J. Schöberl. NETGEN - An advancing front 2d/3d-mesh generator based on abstract rules. *Comput. Visual. Sci.*, 1(1):41–52, 1997.

[22] K. Stüben. An introduction to algebraic multigrid. In U. Trottenberg et al., editor, *Multigrid*. Elsevier Academic Press, 2001.

[23] P. S. Vassilevski. *Multilevel Block Factorization Preconditioners: Matrix-based Analysis and Algorithms for Solving Finite Element Equations*. Springer, 2008.

[24] G. Yang, J. Kabel, B. van Rietbergen, A. Odgaard, R. Huiskes, and S. C. Cowin. The anisotropic Hooke's law for cancellous bone and wood. *Journal of Elasticity*, 53(2):125–146, 1998.